Proceeding of the Korean Nuckear Society Spring Meeting
Kwangju, Korea, May 2002

Optimization of the Flow Distribution Plate of SMART Using Computational Fluid Dynamics

H. S. Kang, S. H. Kim, B. S. Choi, S. Y. Ryu, D. J. Lee

Korea Atomic Energy Research Institute
P.O.BOX 105, Yusung

Abstract

The SMART is an integral type pressurized water reactor with a rated thermal power of 330MWt, currently under development at KAERI (Korea Atomic Energy Research Institute). In SMART design, the uniform distribution of the primary coolant is required at the entrance region of the reactor core. Therefore, the throttling orifices, the comb assembly, and the flow distribution plate (FDP) are installed at the bottom of steam generator (SG) cassettes, the bottom region in the downcomer, and the plenum below the core, respectively. The previous studies on the primary coolant circuit of SMART show that the FDP plays the most important role in the flow distribution in the lower plenum. The shape of the FDP is similar to the honeycomb with many small holes. And also, in general, larger pressure drop induced by the FDP tends to give a more uniform flow distribution in the lower plenum. However, the large pressure drop through the FDP may give adverse effects on the coolant flow during the natural circulation mode, and require more MCP power. Therefore, the design optimization of the FDP is needed to provide the uniform flow distribution with the reasonable pressure drop to the entrance region of the reactor core. Based on the primary system design, 5 cases were selected for the optimization of the FDP. The analysis was performed using computational fluid dynamics code CFX4.4 because the CFD requires less cost and time than the experimental method. The hydraulic resistance value of the FDP may be reduced to 50% of a nominal value, and may be reduced to 75% if the diameter of small hole on the center region in FDP is properly adjusted. These results will be used at the design optimization of the primary coolant circuit of SMART after performing the mechanical structure analysis.

1. Introduction

The SMART is an integral type pressurized water reactor with a rated thermal power of 330MWt. Different from the loop-type reactors, all major primary components are installed in a single pressure vessel, as shown in Fig. 1. The integrated arrangement of these components enables the elimination of large-sized pipe connections between the components of the primary reactor coolant systems, and thus fundamentally eliminates the possibility of large break loss of coolant accidents [1,2]. Table 1 shows the major design parameters of SMART. As shown in the Fig. 1, SMART has twelve identical SG cassettes that are located in the annulus formed by the reactor vessel and the core support barrel. The coolant forced by MCPs enters twelve SG cassettes, and then flows downward to the lower plenum through the downcomer and the comb assembly. The flow direction of the coolant changes to upward at the lower plenum and then flows through the Flow Distribution Plate (FDP) and the reactor core. After passing the core, the coolant circulates through the Support Cylindrical Shell (SCS), the Core Support Barrel (CSB), and finally through the MCP. Since the distance between the MCP outlets and the SG cassettes is a rather large vacant space, the throttling orifices are installed at the bottom of the SG cassettes to obtain the uniform flow distribution through each SG cassette. During the normal operation (four MCPs operation), these orifices ensure the uniform flow distribution of the 12 SG cassettes. However, in case of the emergency operation mode, such as one MCP is stopped, the non-uniform flow distribution of the coolant is formed in the lower plenum [3,4,5,6]. Therefore, the FDP and the comb assembly, Fig. 2, are installed to obtain the uniform coolant flow moving to the core region by imposing additional hydraulic resistance. The shape of the FDP is similar to the honeycomb with many small holes. And also the comb assembly located at the bottom region of the downcomer filters debris in primary system. The design parameters of the FDP and the comb assembly are summarized in Table 2 and 3. In general, larger pressure drop induced by the FDP and the comb assembly tends to give more uniform flow distribution in the lower plenum, but it increases the total flow resistance of the primary system. The previous studies on the primary coolant circuit of SMART show that the FDP plays the most important role on the flow distribution in the lower plenum [7,8], and the present design value, 16 KPa of pressure drop at normal operation condition, of the FDP sufficiently assure the uniform flow distribution at the entrance region of the reactor core. However, this value is a little bit large pressure drop compared to the total pressure drop of the primary circuit. And this increased flow resistance requires more MCP power and may cause adverse effects on the coolant flow during the natural circulation mode. Therefore, the design optimization of the FDP is needed to minimize the system resistance within ensuring the uniform coolant flow field. This study was performed as part of the design optimization of the primary coolant circuit of SMART. Based on the primary system design, 5 cases were selected for the optimization study including different hole diameter depending on the region of the FDP. The analysis was performed using computational fluid dynamics code CFX4.4.

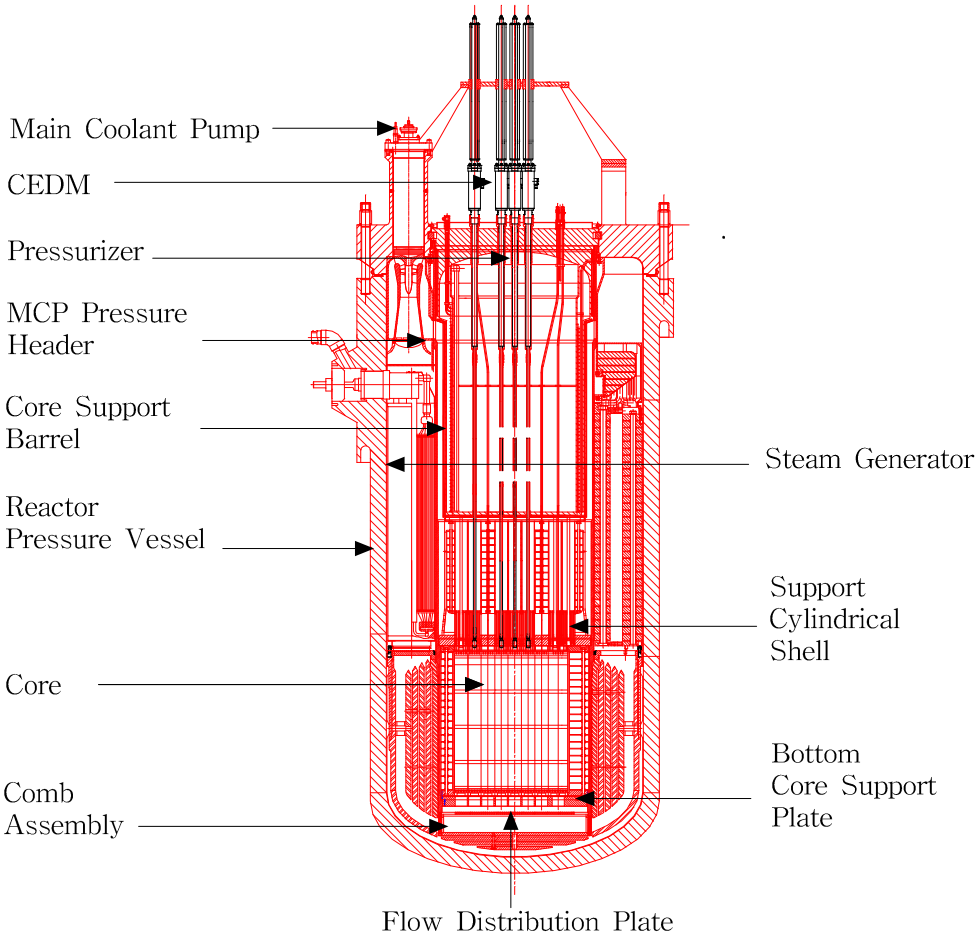

Fig. 1 SMART Vessel Assembly

Table 1. Major Design Parameter of SMART[1,2]

Thermal Power of the Reactor	330 (MWt)
Pressure in Primary Circuit Nominal/Design	15.0/17.0 (MPa)
Coolant Temp. Rise at Core	40.0 (℃)
Coolant Flow Rate via the Core	1550.0 (kg/s)
Number of MCPs	4
Steam Output (kg/s)	152.4 (kg/s)

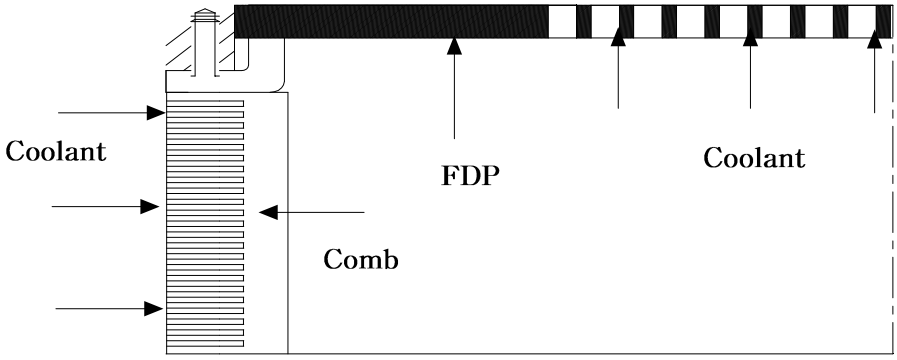

Fig. 2 The Geometry of the FDP & Comb Assembly{1,2]

Table 2. Design Parameters of FD Plate [1,2,10]

Flow Distribution Plate		
Number of Hole	3200	-Pressure Drop at Normal Operation : 16 KPa -Idelchik Handbook : 8-3 model
Dia of Hole (mm)	20	
Dia. of Plate (mm)	2081	
Thick. of Plate (mm)	30	

Table 3. Design Parameters of Comb Assem. [1,2,10]

Design Parameter of Comb Assembly		
Number of Solid Plate in Axial Direction	24	-Pressure Drop at Normal Operation: 0.958 KPa -Idelchik Handbook: 4-1, 4-9 model
Height of Comb (mm)	240	
Height of Solid Plate (mm)	5×22 7×1 8×1	
Solid Plate Fraction in Axial Direction	0.52	

Table 4. Cases Studies for FDP Optimization

Case	Operation Mode	Flow Distribution Plate
Case 1	4MCP, 100%[1]	Nominal △P
Case 2	3MCP*, 75%[1]	Nominal △P
Case 3	3MCP, 75%	△P(Case 2)/2
Case 4	3MCP, 75%	△P(Case 2)/4
Case 5	3MCP, 75%	△P(case2)/4 with 25% increased flow area of center region in FDP (Fig. 3)

* 3MCPs Op. : When One MCP is stopped
1 : 100%, 75% Reactor Power Operation

2. Numerical Aanlaysis

2.1 Grid Model Generation

A multi-grid quarter symmetric model, simulating the outlets of SG cassettes, downcomer, combs, FDP, core, and CSB was constructed to calculate the flow field of the primary system, especially in the lower plenum (Fig. 3). The radiation shield plates in the downcomer region are modeled by the solid patch option in CFX4.4 command file. Five shield plates are modeled as three plates that maintain the effective flow area. The 24 solid plates in the comb are also modeled as 6 plates using effective flow area. The FDP, BCSP, core, and SCS are modeled as a porous medium based on the effective flow area and the pressure drop induced by the geometrical change and frictional loss. The volume porosity and the pressure drop of the porous mediums are shown in Tables 2, 3 and 5. The number of cells in this grid model is 224,560 cells.

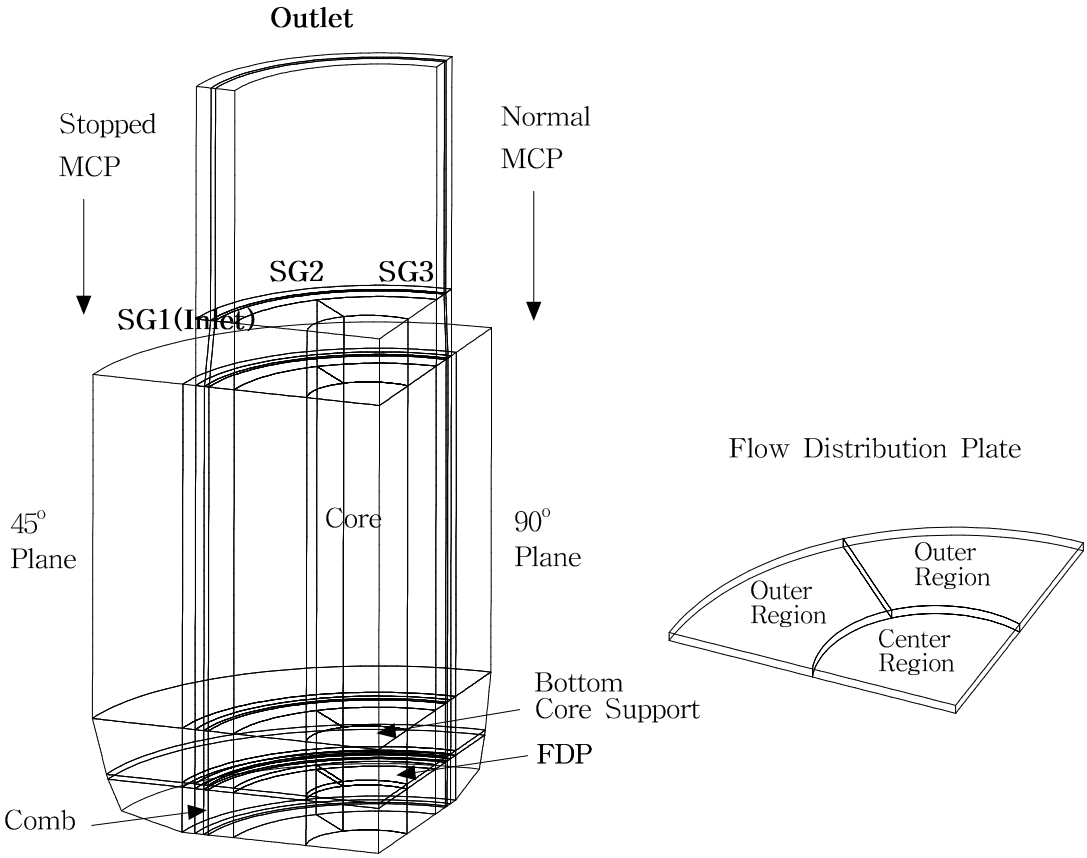

Fig. 3. The Grid Model

Table 5. Volume Porosity and Pressure Drop

Porous Medium	Volume Porosity	Pressure Drop (KPa)	Source
FDP	0.34*	16.0	Idelchik, 8-3
BCSP	0.48	0.95	Ref. [1,2]
Core	0.48	9.53	Ref. [1,2]
SCS	0.258	15.0	Idelchik, 11-15

*: In case 5, the porosity of the center region in FDP was increased to 0.425

2.2 Governing Equations

The flow and pressure field is modeled by the incompressible three dimensional Navier-Stokes equation with the standard k-ε turbulence model included in the CFX4.4 [10]. The governing equations used in this study are written in coordinate free tensor notation as follow.

$$\nabla \cdot (\rho V) = 0 \tag{1}$$

$$\nabla \cdot (\rho V \otimes V) - \nabla \cdot (\mu_{eff} \nabla V) = -\nabla P + \nabla \cdot (\mu_{eff} (\nabla V)^T) + B \tag{2}$$

$$B = B_F - (R_C + R_F |V|) V \tag{3}$$

$$\nabla \cdot (\rho V k) - \nabla \cdot ((\mu + \frac{\mu_T}{\sigma_k}) \nabla k) = P + G - \rho \varepsilon \tag{4}$$

$$\nabla \cdot (\rho V \varepsilon) - \nabla \cdot ((\mu + \frac{\mu_T}{\sigma_\varepsilon}) \nabla \varepsilon) = C_1 \frac{\varepsilon}{k} (P + C_3 \max(G, 0)) - C_2 \rho \frac{\varepsilon^2}{k} \tag{5}$$

$$\mu_{eff} = \mu + \mu_T, \qquad \mu_T = C_\mu \rho \frac{k^2}{\varepsilon} \tag{6}$$

$$P = \mu_{eff} \nabla V \cdot (\nabla V + (\nabla V)^T) \tag{7}$$

2.3 Boundary Condition and Modeling of Porous Medium

The inlet boundary conditions were set at the SG outlets for the velocity, k, and ε, and the outlet boundary conditions were set at the MCP inlets with a pressure reference value. The symmetric condition is applied to the 0^o and 90^o cut surface, and no-slip condition is used at the wall. The parameters used for boundary conditions are shown in Table 6. The volume porosity for each porous medium can be determined using the relationship between the effective flow area in the SMART and the physical area in the grid model. The body forces "B" are added to the momentum equation (2) as shown in equation (3). The speed-factor, R_F, is introduced, to include the flow resistance due to the local velocity. The relationship between the speed-factor, R_F, and flow resistance coefficient, ζ, used in this study is as follows [10,11].

$$R_F = \zeta \frac{A}{V} \frac{\rho}{2} \tag{8}$$

The values for flow resistance were taken from the design document of SMART and the handbook of hydraulic resistance [1,2,11,14].

Table 6. Inlet & Outlet Boundary Condition [1,2,10]

	Inlet Condition(Velocity, m/s)		Outlet Pressure Condition
	4 MCP	3 MCP	
SG 1	0.964	0.748	-0 Pa *inlet value : $k_{in}=0.002V_{in}^2$ $\varepsilon_{in}=k_{in}^{1.5}/(0.3\times D_h)$
SG 2	0.964	0.646	
SG 3	0.964	0.612	

In case 5, the volume porosity of the center region in the FDP (Fig. 3) is only changed to the 25% increased value of the nominal one to consider the flow area variation (Table 4).

2.4 Calculation Method

The steady state computation for each case was conducted with a small under-relaxation factor, 0.25, for velocity, k, and ε. The algebraic multi-grid solver for velocity, k, and ε was also used to obtain a good converged solution. The mass residual was set to 1×10^{-4}. The number iteration for each steady computation was in the range of 6,000~8,000.

3. Results and discussions

Fig. 4 and 5 show the velocity vector profile, velocity contours, and total pressure distribution of the SMART primary system from the SG cassettes outlets to the MCP suction for the case 1. As shown in Fig. 4. (a), the coolant entering through the inlet flows downward to the bottom region in the downcomer, and passes through the comb assembly as a jet form due to the rapid reduction and expansion in flow area (Fig. 4. (b), "A"). The flow area is decreased about 50% in the region of the comb assembly from the front region of it. After passing the comb assembly, the coolant quickly moves to the center region below the FDP, and turns its direction in the upward. At this point, as the coolant mainly moves upward along the left region, this flow pattern makes the flow distribution below the FDP non-uniform. But the coolant almost uniformly flows into the entrance region of reactor core after passing the FDP (Fig. 4. (b), "B"). This is because the large pressure drop, about 16 KPa, take place when the coolant passes the FDP makes the uniform flow distribution of coolant in the FDP downstream. The velocity contours along axial direction in the lower plenum are shown in Fig. 4. (c), (d), (e), and (f). We can see that the flow distribution becomes uniform after the coolant passes the FDP. As shown in these figures, the maximum velocity difference below the FDP was about 1.0 m/s (Fig. 4. (d)), but the maximum velocity difference above the FDP was about 0.3 m/s (Fig. 4. (f)). In this evaluation, the velocity

contours, the boundary of the outside region, due to no-slip condition in the near the wall are neglected. The total pressure distribution along the 0^{o} plane, and just below and above the FDP is shown in the Fig. 5. (a), (b), and (c). According this figure, we can see that the pressure drop imposed by the boundary condition of the momentum sink is well calculated, and considerably agree with the system parameter (Table 5). For the comb assembly, the simplified real geometry modeling instead of the momentum sink condition was used to calculate the pressure field. The total pressure distribution around the comb assembly shows that about 1KPa of pressure drop develops when the coolant passes it. This is a good agreement with the value of 0.95 KPa incited from the handbook of hydraulic resistance.

In case 2, the magnitude of velocity difference above the FDP is also greatly reduced to about 0.2 m/s, as shown in Fig. 6. The pressure drop due to the FDP is decreased to 7KPa as the coolant flow rate is reduced from 384 kg/s to 266 kg/s for 3 MCPs operation. The contours below the FDP in case 2 show to be more asymmetric than that of the case 1. It is because the different inlet velocity profiles through SG 1, 2, and 3 directly affect the flow field below the FDP so that the secondary flow occurs at around 0^{o} plane in center region under the FDP. But this asymmetric velocity contour disappears after the coolant passes the FDP.

In case 3, the pressure drop of the FDP is reduced to 50% of the case 2 by adjusting the momentum sink condition of the FDP. As shown in Fig. 7, the velocity contours above the FDP are very similar to those of case 2, but less uniform than that of case 2. This implies that the FDP design can be modified to reduce the hydraulic resistance with ensuring the uniform flow distribution. The results of case 4, simulating 75% reduced the pressure drop of a nominal value, are shown in Fig. 8. The magnitude of velocity difference above the FDP is about 0.25 m/s, and rather similar to that of case 2 and 3. However, the variation of velocity (Fig. 8. (b)) is a little bit larger than that of case 2 and 3. Therefore, the idea of increasing the flow area of center region of the FDP (case 5) is derived to reduce this variation with maintaining the FDP pressure drop of case 2. The increased flow area is about 25% of nominal value, and also is reflected by increasing the volume porosity value. As shown in Fig. 8, the velocity variation (Fig. 9. (b)) is a little bit reduced, and almost similar to that of case 4. From this calculation results, we can see that 50~75% reduced pressure drop of a nominal value and the increased flow area of center region of the FDP can provide the uniform flow distribution into the entrance region of reactor core.

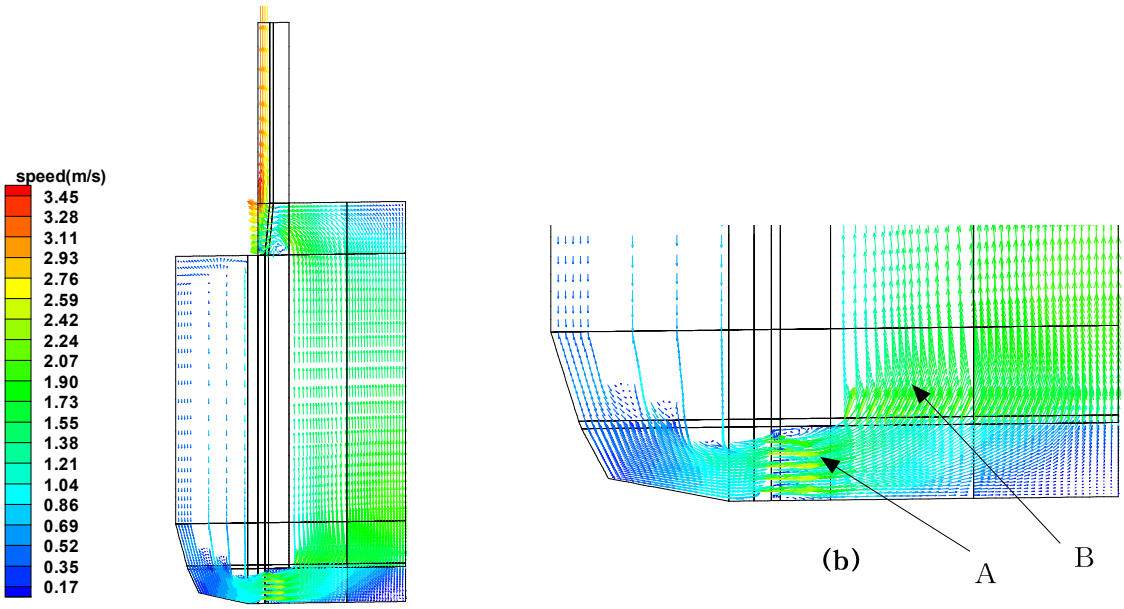

(a) Velocity Profile on the 0° Plane

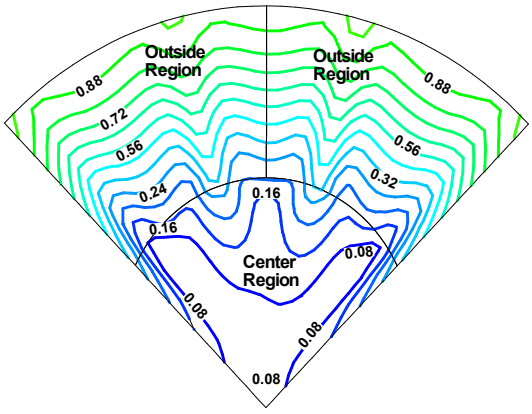

(c) Velocity Contours at 2cm above Bottom (m/s)

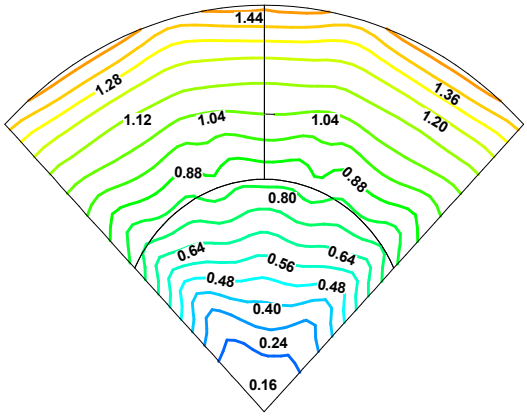

(d) Velocity Contours at 14.5cm above Bottom (m/s)

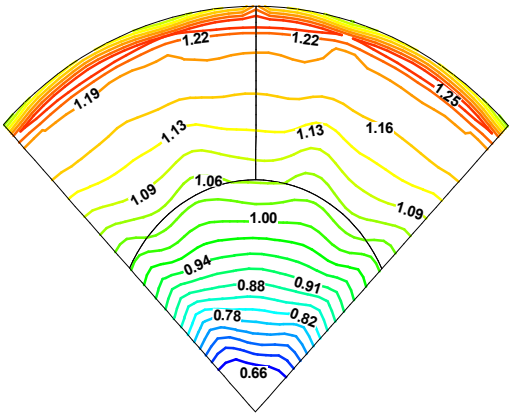

(e) Velocity Contours at 27cm above Bottom (m/s)

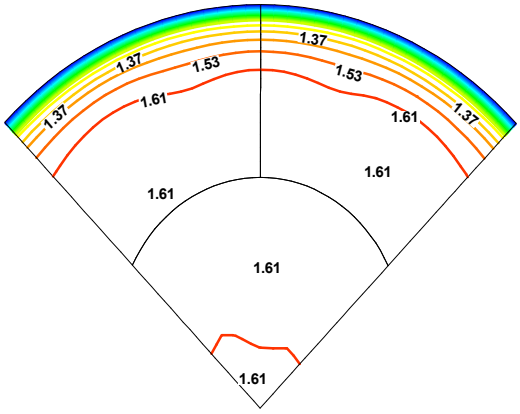

(f) Velocity Contours at 5cm above FDP (m/s)

Fig. 4. Velocity Profile and Contours in Case 1

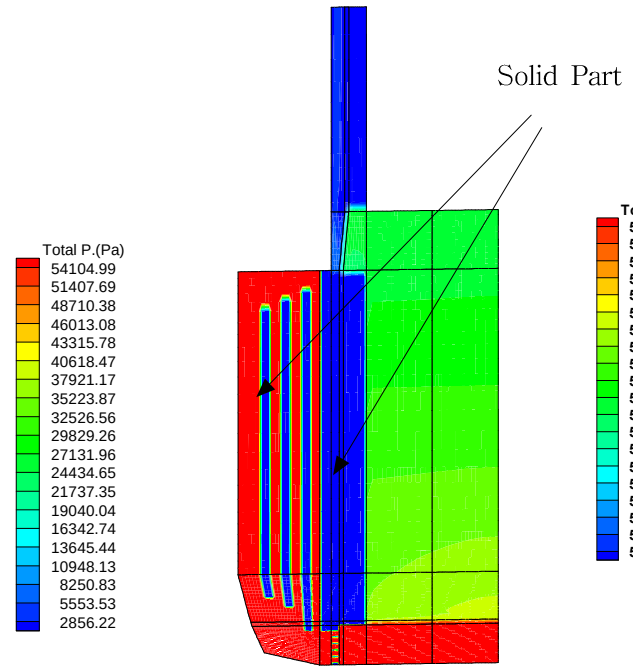

(a) Total Press. on the 0° Plane

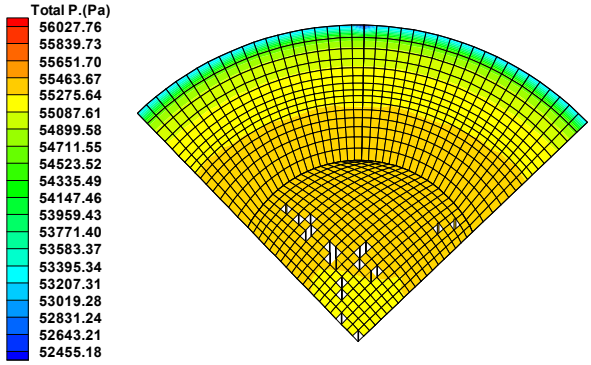

(b) Total Press. below FDP

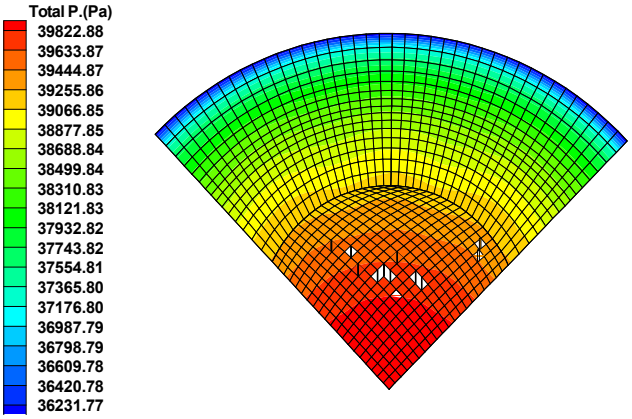

(c) Total Press. above FDP

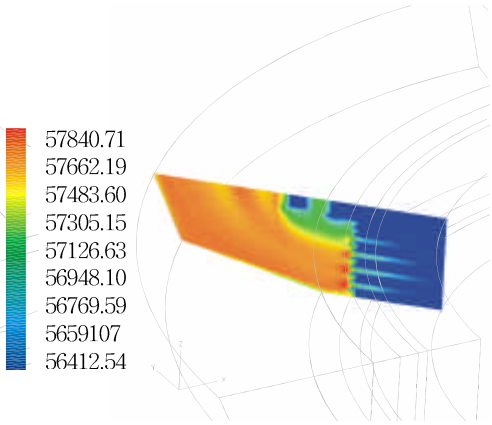

(d) Total Press. around Comb Assem. on the 45° Plane

Fig. 5. Total Pressure Distribution in Case 1

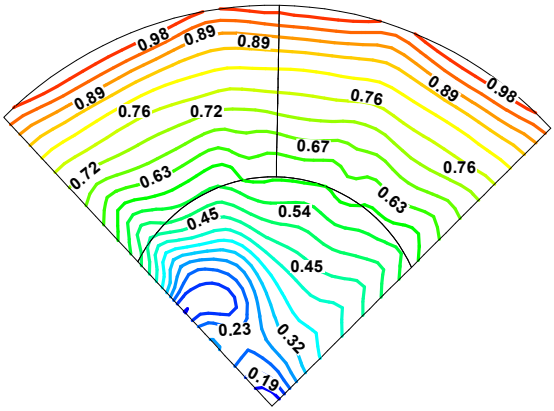

(a) Velocity Contours at 14.5cm above Bottom (m/s)

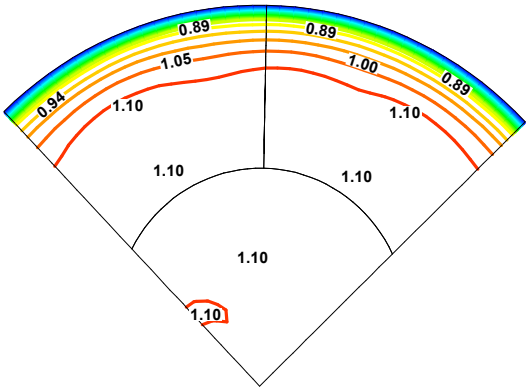

(b) Velocity Contours at 5cm above FDP (m/s)

Fig. 6. Velocity Contours in Case 2

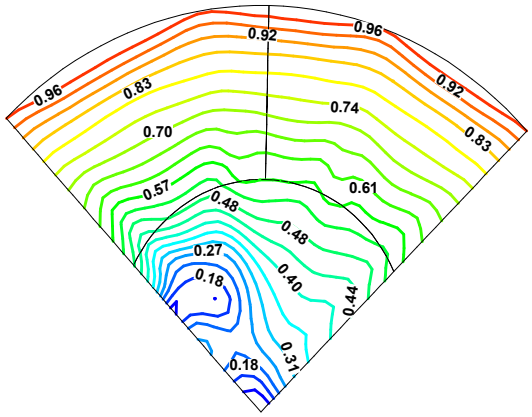

(a) Velocity Contours at 14.5cm above Bottom (m/s)

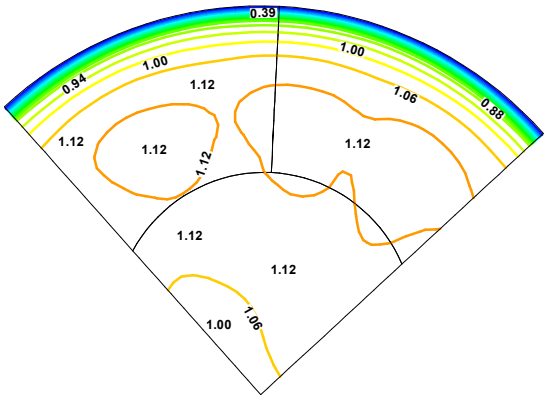

(b) Velocity Contours at 5cm above Bottom (m/s)

Fig. 7. Velocity Contours in Case 3

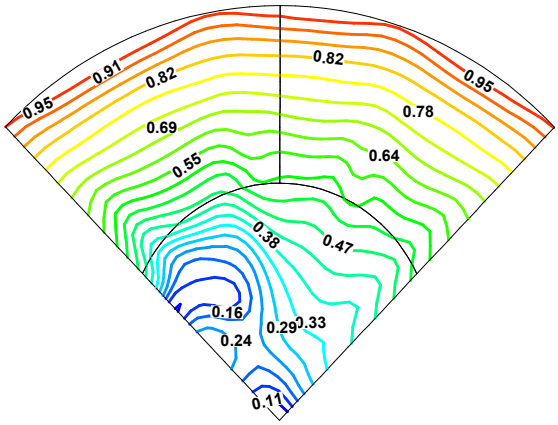

(a) Velocity Contours at 14.5cm above Bottom (m/s)

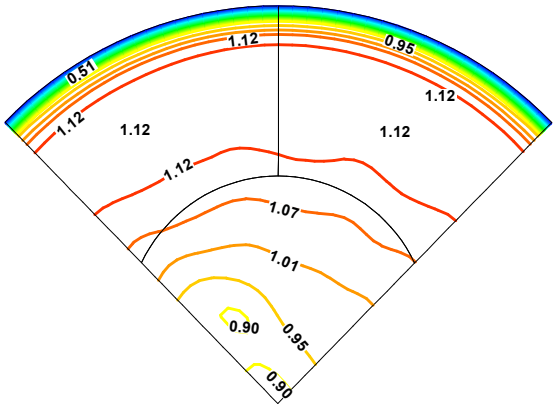

(b) Velocity Contours at 5cm above Bottom (m/s)

Fig. 8. Velocity Contours in Case 4

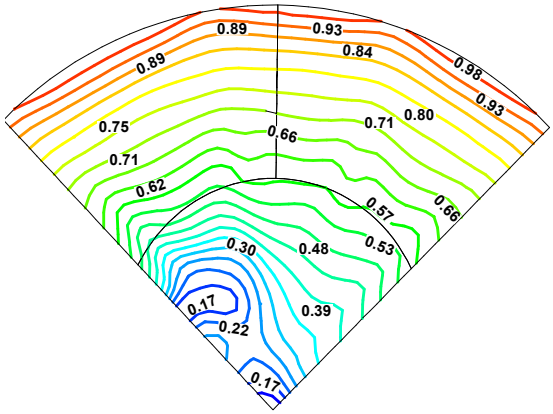

(a) Velocity Contours at 14.5cm above Bottom (m/s)

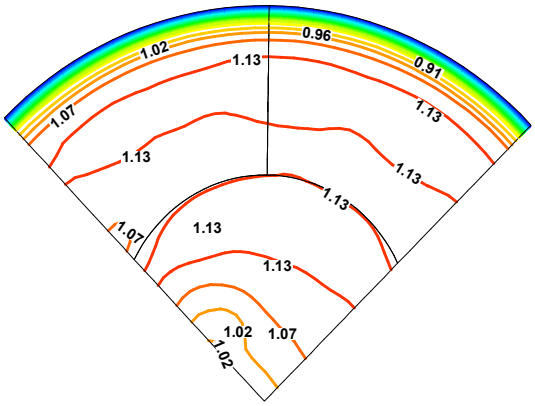

(b) Velocity Contours at 5cm above Bottom (m/s)

Fig. 9. Velocity Contours in Case 5

4. conclusions and future work

The analysis results using CFD show that the preliminary design of the FDP of SMART enoughly provides the uniform flow distribution into the entrance region of the reactor core for the normal operation (four MCPs operation) and the emergency operation mode such as one MCP stopped operation. And the results of various cases for the FDP optimum design show that the hydraulic resistance of the FDP may be reduced to the 50% of a nominal value, and reduced to the 75% values with 25% increased the flow area of the center region in the FDP. This recommends that the diameter of small hole in the FDP is differently designed to provide the optimum flow conditon into the entrance region of reactor core. These results will be used at the design optimization of the primary coolant circuit of SMART after performing the mechanical structure analysis. As a future work, if it is possible, the porous media modeling about the FDP will be changed to the real geometrical modeling, and also the geometrical modeling the 57 fuel assemblies will be carried out to obtain the better information of reactor core flow.

Acknowledgments

This study has been carried out as a part of the Development of Design Technology for Integral Reactor program supported by Ministry of Science and Technology. The authors are sincerely grateful for the financial support.

References

1. H. Y. Kim, et al, System Description of SMART , Technical Report, SMART-FS-SD210, Rev. 00, KAERI, 1998.

2. D. J. Lee, et al, Development of Fluid System Design Technology for Integral Reactor , Technical Report, KAERI/RR-1883/98, KAERI, 1999.

3. H. S. Kang, and Y. Y. Bae, Studies on Thermal Hydraulic Characteristics of Flow through MCP Pressure Header and Lower Plenum depending on SMART Operation Modes , Technical Report, KAERI, 1998.

4. H. S. Kang, et al, Effect of MCP Pressure Header on Coolant Mass Flow Distribution among SG Cassettes in the SMART , Proceedings, 98 Spring Korea Nuclear Society Conference, Vol. 1, PP. 617-622, 1998.

5. H. S. Kang, et al, A Numerical Study on the Optimum Size for the Orifice Located on the

Steam Generator Cassette of Integral Reactor , Proceedings, 98 Spring Korea Computational Fluid Dynamic Conference, Vol.1, PP. 75-81, 1998.

6. H. S. Kang, et al, A Study on the Thermal Hydraulic Characteristics of Flow in the Primary System of SMART Depending on the Operation modes , Proceedings, ICONE-8 Conference, 2000.
7. H. S. Kang, Y. D. Hwang, and D. J. Lee, Numerical Analysis of the Lower Plenum Flow Field for SMART , Proceedings, CFD2001 Conference, 2001

8. H. S. Kang, Y. D. Hwang, and D. J. Lee, A Study on the Lower Plenum Flow Field of SMART using CFX Code , Proceedings, 01 Autumn Korea Nuclear Society Conference, 2001.

9. I. E. Idelchik, Handbook of Hydraulic Resistance , Second Edition, Hemisphere Publishing Corporation, 1986.

10. CFX4.4 User Manual, AEA Tec., 1999

11. T. Hohne, Coolant Mixing in Pressurized Water Reactors , Proceedings, ICONE-7 Conference. 1999

12. K. B. Park, et al, Development of Mechanical Design Technology for Integral Reactor , Technical Report, KAERI/RR-1888/98, KAERI, 1999.